Materials Science-Poland, 41(2), 2023, pp. 227-243
http://www.materialsscience.pwr.wroc.pl/
DOI: 10.2478/msp-2023-0019

Investigation of the mechanical, corrosion, and tribological characteristics of AZ61 Mg with boron carbide nano particles via the stir casting route

S. Sakthi[1,*], S. Mahendran[1], M. Meignanamoorthy[2], V. Mohanavel[3]

[1]Department of Mechanical Engineering, University College of Engineering, Thirukuvalai-610204, Tamilnadu, India
[2]Department of Mechanical Engineering, Chendhuran College of Engineering and Technology, Lena Vilakku, Pudukkottai – 622507, Tamilnadu, India
[3]Centre for Materials Engineering and Regenerative Medicine, Bharath Institute of Higher Education and Research, Chennai – 600073, Tamilnadu, India

Magnesium composites are innovative, compact, and distinctive materials. Because of their low density, magnesium composites are suitable for applications in the automobile, aviation, semiconductor, and pharmaceutical sectors. To enhance the mechanical wear and corrosion behavior of theAZ61 Mg alloy, different weight percentages of nano-B_4C reinforcements (2.5, 5, 7.5, and 10wt%) were strengthened with magnesium matrix. Fabrication of magnesium composites was achieved through the stir casting method. The as-cast specimens were subjected to microstructural analysis, which showed that the B_4C nanoparticles were dispersed uniformly, well bonded to the matrix, and had a minimal level of porosity. This shows that the inclusion of B_4C nanoparticles has aninsignificanteffect on the microstructure of the as-cast material. The material's tensile strength, compressive strength, hardness, corrosion resistance, and wear resistance were all greatly increased by the Mg17Al12 phase's fracture and dispersion. Scanning electron microscopy was utilized to inspect the surfaces of AZ61/B_4C nanocomposites and witnessed the uniform dispersal of reinforcement within the matrix.The maximum value for mechanical properties was obtained for AZ61/7.5wt%B_4C nanocomposite and the lowest value was found to be the corrosion test. These results show that the AZ61/7.5wt%B_4C nanocomposite is a superior material for aerospace and automotive engineering components where high compressive strength, corrosion resistance, and wear resistance are required.

Keywords: *AZ61/B_4C nanocomposite, mechanical properties, corrosion behavior, stir casting, tribological characteristics, Grey Taguchi technique*

1. Introduction

Magnesium-related alloys appear to possess-less density, highly specialized automatic properties, and outstanding damping behavior. Because of these characteristics, they have significant implementation potential in aerospace and the automotive industry, two fields in which material weight reduction is critical. Magnesium and its composites are not utilized in the field of engineering despite their less mechanical behavior [1–4]. These characteristics include strength, ductility, a low elastic modulus, and poor stability at high temperatures. In this respect, metal matrix composites of magnesium, which are also known as Mg-MMC, have ceramic reinforcement in the form of fibers or particles, and as a result, they are stronger at higher temperatures and have better hardness, wear resistance, and elastic modulus. Nevertheless, the use of ceramic reinforcements in pure Mg and Mg alloys can lead to brittle materials [5–8]. In recent years, metallic elements with high strength and modulus, such as titanium, nickel, and copper, have been introduced to improve the mechanical properties of pure magnesium and its alloys [9–11]. When 5.6 wt% of titanium, which is insoluble in magnesium, was added to pure magnesium, it was reported that there was an overall increase in ductility of 45% and a yield strength of 60% [12]. While soluble metallic elements such as Ni and Cu were added to pure Mg, the strength of the material signifi-

* E-mail: sakthi.mech1990sss@gmail.com

cantly improved, but its ductility significantly decreased [13]. On the other hand, it has been reported that adding nanosized ceramic reinforcements to magnesium and its alloys (such as Al_2O_3, ZrO_2, or ZnO) resulted in an increase in both the material's overall strength and ductility [14, 15]. Stir casting isutilized to manufacture magnesium matrix composites [16–22]. These composites use silicon-carbide-reinforced particles. A variety of particles of various sizes, including micron, submicron, and nanometer-sized particles were used. In the course of the research, it was found that stir casting and extrusion processes were the most active ways to increase the strength of the magnesium composite. It was discovered that the accumulation of SiC particles of varying sizes led to a direct improvement in the dynamic recrystallization (DRXed) nucleation ratio. Similarly, it can reduce the average particle size of the matrix. Compared to the state in which no SiC material was added, the tensile strength of the composites exhibited a noteworthyenhancement. The mechanical properties of aluminum alloys may be enhanced using a stir casting process to incorporate nanoscale B_4C composites [23–27]. Microstructure analysis revealed the presence of boron carbide nanoparticles that had disseminated throughout the aluminum alloy in the pristine condition. The mechanical properties' tensile strength and hardness were enhanced as the amount of boron carbide nanoparticles in the material increased. They found that the wear opposition of B_4C nanocomposites was significantly greater than that of monolithic aluminum alloys [28–30]. The tribological characteristic of deformed AZ61 alloy was explored, and the wear loss of rolled specimens was found to be better than that of extruded specimens [31]. The wear loss of AZ61/SiC composites was investigated and SiC-reinforced AZ61 composites were observed to possess better wear resistance than the matrix [32]. The number of grains in a microstructure was calculated, and the ASTM grain size of Mg alloys was determined using computer vision technology. The success rate in the comparison of the grain numbers was found to be approximately 94% [33]. The tribological behavior of magnesium-strengthened fly ash cenosphere was studied, resulting in the conclusion that increasing reinforcement improved wear resistance [34]. The wear properties of SiC-strengthened magnesium composites were examined, and it was observed that inclusion of SiC reinforcement leads to better wear opposition [35]. The mechanical and wear characteristics of nano-fly ash particle reinforced Mg matrix composites produced via stir casting process were examined, and it was found that the addition of nano-fly ash particle enhances the mechanical and wear properties significantly [36]. The mechanical behavior of ceric ammonium nitrate reinforced magnesium was tested and an increase in ceric ammonium nitrate was found to improve mechanical behavior [37].

Numerous publications reveal that composites based on magnesium with reinforcements, such as silicon carbide and aluminum oxide, can improve the mechanical properties of the material. And also help in investigating the influence these particles have. However, few examples of Mg-based MMCs with nano-B_4C mechanical, tribological, and corrosion properties can be found in the scientific literature.

This comprehensive literature review has focused on the area of nano-B_4C -reinforced AZ61 Mg composites produced via the stir casting process. On the basis of the literature review, an effort has been made to produce Mg AZ61/B_4C nanocomposites using the stir casting process in order to study the surface morphology and mechanical, tribological, and corrosion behavior. The influence of nano-B_4C (different weight percentages 2.5 wt%, 5 wt%, 7.5 wt%, and 10 wt%) reinforced with AZ61 Mg properties were studied and the results are provided in this report.

2. Visual examination

In the detailed literature study on magnesium matrix composites, numerous research gaps were identified in the areas of the manufacturing of magnesium matrix composites via the stir casting process, their characterization, their physical properties, and in their mechanical, tribological, and corrosion behavior, all of which are enumerated below. Numerous investigations have been carried out on the synthesis of magnesium matrix composites

via the stir casting process, but very little work was done by using AZ61 Mg alloy as a matrix material and nano-B_4C as the reinforcement. Very few researchers have studied the tribology and corrosion behavior of the magnesium matrix composites.

3. Materials and experimental methods

Mg-Zn master alloys were utilized to create magnesium alloy AZ61 in a high-frequency induction furnace with a protective atmosphere containing 5% SF6.This preparation was made under protective gas conditions. In the first stage of the melting process, pure Mg was loaded into a graphite-ceramic crucible. This allowed the Mg to melt. Subsequently, AZ61 magnesium alloys were added to the molten magnesium and mixed until they were completely dissolved in the molten magnesium (which had been heated to 800°C). The matrix alloys and their elemental compositions are 6.73wt% of Al, 1.0wt% of Zn, 0.03wt% of Si, 0.003wt% of Cu, 0.0035 wt% of Fe, 0.0007wt% of Ni, with the remaining weight percent consisting of Mg. Using the stir casting method, pure B_4C nanoparticles with an average size of 90nm were introduced into the molten alloy to prepare the composite for the ex-situ process. As a reinforcing element, B_4C nanoparticles were preheated by being held at a temperature of 400°C for two hours. An induction furnace was used for the stir-casting process, and a steel impeller was used to add different amounts of preheated B_4C nanoparticles (2.5wt%, 5wt%, 7.5wt%, and10wt%) to the molten state of the AZ61. The temperature of the molten AZ61 was 780°C.

The stir casting procedure was performed at a stirring speed of 620rpm for a period of 15min. Before adding B_4C nanoparticles to the molten alloy at 780°C using the vortex method, they were preheated at 400°C for 120min. The pouring temperature was kept under control with the help of an accurate K-type thermocouple in each trial. Finally, the molten composites were poured at 750°C into a cast iron mold that was preheated to a temperature of 100°C.

Figure 1 shows the manufactured composites. To expose the microstructures, each of the cast samples was subjected to a process that involved polishing and etching with an acetic picric solution (10 ml H_2O+10ml ethanol+10ml acetic acid+4.2g picric acid). The polishing was done using disc polishing machine to obtain a mirrorlike surface. Then, it was etched using acid. After the etching process, elemental and micro structural analyses were performed using energy dispersive spectroscopy (EDAX-AMETEK-TSL model) and scanning electron microscope (ZEISS model).

According to ASTM standards D695 and D3039, compression and tensile test samples were prepared using a wire-cutting machine. These samples were then machined to the appropriate dimensions for the compression test: 8mm in diameter and 12mm in height. Compression and tensile tests were performed at room temperature at a constant speed of 0.1mm/min for the crosshead. A computer-controlled UTM 50kN was used to perform the compression and tensile test. According to ASTM International Standard E384, a Vickers indenter with a test load of 0.5kg and dwell time of 30s was used with an automatic digital microhardness tester to measure the hardness of the polished as-cast materials. The examination was performed at room temperature, and hardness measurements were collected from five distinct locations across each composite material. The Charpy V-notch test was used to determine the toughness of the composites in accordance with ASTM E23. Each specimen had a single V-Notch that was 2mm deep and 45° in angles with a root radius of 0.1mm. The size of the specimens was 10mm × 10mm × 55 mm. The Charpy V-notch test was performed using an impact test machine. According to ASTM International Standard C1161, a flexural test was conducted to measure the flexural strength of the material. A computer-controlled UTM was used to perform the three-point bend test, with a constant displacement rate of 0.5mm/min.

According to ASTM International Standard B117, Versa STAT MC (potentiostat/ galvanostat with a versa studio electrochemistry software package, Princeton Applied Research, Princeton, New Jersey) was used to perform an electrochemical

analysis of the samples. At room temperature, polished magnesium composites with a surface area of 1cm^2 were subjected to a corrosion medium consisting of a 3.5% sodium chloride solution. The dynamic current–potential curves were recorded by polarizing the specimen to −0.1 V to +0.1 V on open circuit potential (OCP) at a scan rate of 0.05 mV/s. Platinum as counter electrode and saturated calomel as reference electrode were used.

To carry out the wear test such as wear rate and co-efficient of friction on the produced nanocomposites, they were cut into the required dimensions as per ASTM standard E99, with a 10mm × 30mm cylindrical pin, using a wire electric discharge machine. A DUCCOM pin on a disc tribometer was used to perform the test. The disc plate was polished with acetone to obtain a smooth finish and remove impurities present on the disc. The wear test was done at process parameters such as weight percent (0, 2.5, 5,and7.5), load (4N, 8N, 12N, and 16N), sliding velocity (1m/s, 2m/s, 3m/s, and 4m/s), and sliding distance (400m, 800m, 1200m, and 1600m).

4. Results and discussion

4.1. Scanning electron microscope and energy-dispersive X-ray spectroscopy analysis (EDS)

Scanning electron micrographs (SEM) of the AZ61/B_4C nanocomposites are in Figure 2 (a–e). This demonstrates the fact that correct metallographic testing was used to evaluate the structure of the composites. When the weight percent of B_4C was increased, the amount of intermetallic $Mg_{17}Al_{12}$ was slightly reduced [38, 39]. The dendritic features of magnesium can be seen in the matrix of the AZ61/B_4C nanocomposites, and these features can be seen in the microstructures of the composites as well. Figure 2 (b, c) illustrates in detail the equal distribution of augmentations in the

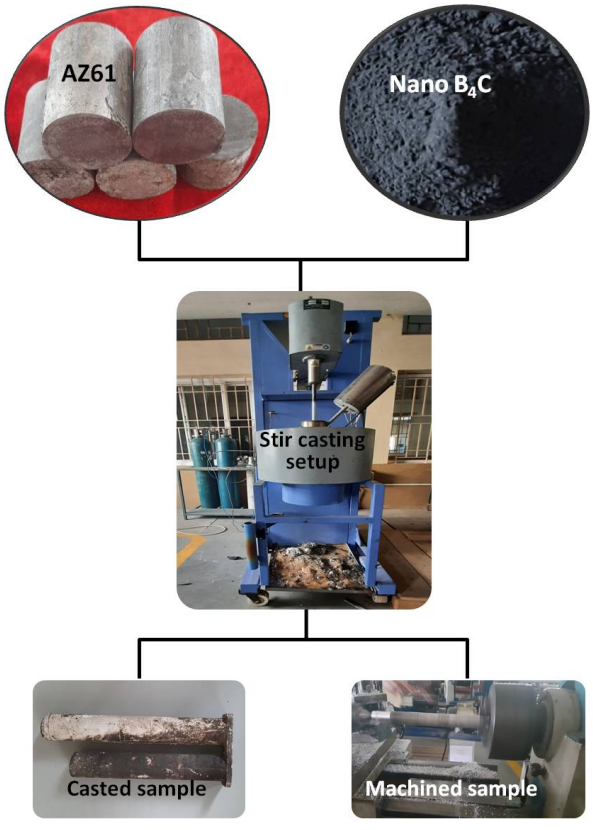

Fig. 1. Fabrication of AZ61/ B_4C nanocomposites

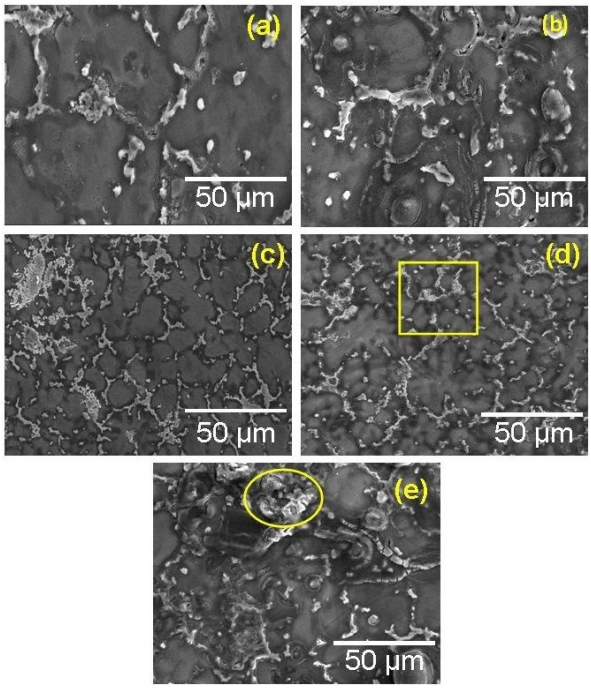

Fig. 2. SEM micrographs of nanocomposites of AZ61/B_4C: (a) AZ61 alloy, (b) AZ61/2.5wt%B_4C, (c) AZ61/5wt%B_4C, (d) AZ61/7.5wt%B_4C, (e) AZ61/10wt%B_4C

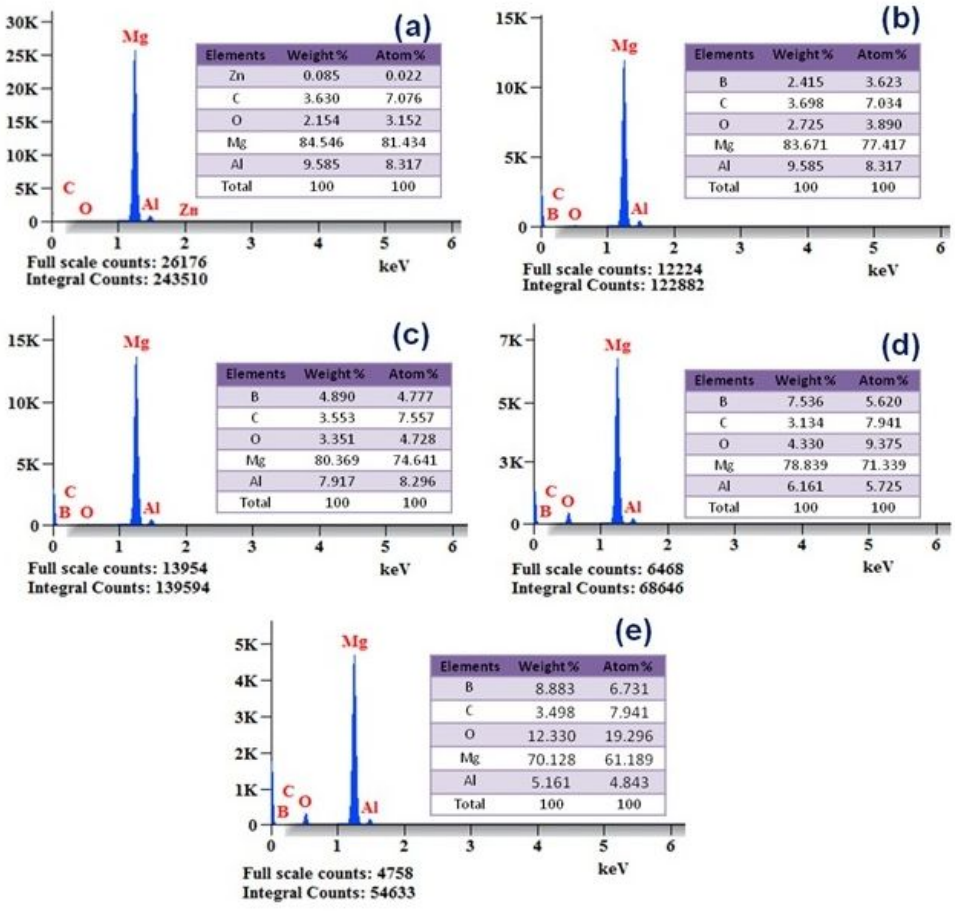

Fig. 3. EDS analysis of nanocomposites of AZ61/B_4C: (a) AZ61 alloy, (b) AZ61/2.5wt%B_4C, (c) AZ61/5wt%B_4C, (d) AZ61/7.5wt%B_4C, (e) AZ61/10wt%B_4C

AZ61 grain limitations and the lack of sponges produced as a result of a properly stirred casting process. This is clear from the intensity of the respective peaks in each of the EDS analyses, as shown in Figure 3. Owing to the isothermal heat reaction that occurs between the matrix and reinforcements, Figure 2 (e) depicts a cluster of reinforcements in the AZ61 matrix of the 10 wt% B_4C nanocomposites. Figure 3 shows the EDS analysis results of the AZ61/B_4C nanocomposites. The results show peaks corresponding to the presence of Mg, Al, and other minor elements. The presence of the B peaks, which can be seen in Figure 3 (c, d), unequivocally demonstrates that an increased weight percentage of nano-B_4C can be found in the alloy. In Figure 3 (b, c, d), the weight percentage of boron B and carbide C are clearly presented, and the presence of both boron and carbide are proven. In addition, boron B and carbide C peaks are clearly displayed in Figure 3 (b, c, d).

4.2. Physical properties

As shown in Table 1, the reinforcement additionin the matrix enhanced the density of the composite material. The density of the samples was determined by calculating the volume of a given sample from its dimensions and then dividing this into the mass.

$$\text{Density, } \rho = m/v \text{ (gm/cc)}$$

The porosity of the composite is calculated using following equation

$$\text{Porosity} = \frac{\rho\text{th} - \rho\text{ex}}{\rho\text{th}} \times 100$$

Table 1. The density of AZ61/B_4C nanocomposites

Composites	Experimental density g/cm^3	Theoretical density g/cm^3	Porosity %
A (AZ61-Mg alloy)	1.785	1.790	1.38
B (AZ61 with 2.5wt% B_4C)	1.801	1.824	1.24
C (AZ61 with 5wt% B_4C)	1.814	1.831	1.18
D (AZ61 with 7.5wt% B_4C)	1.826	1.840	1.07
E (AZ61 with 10wt% B_4C)	1.830	1.848	1.04

Table 2. Tensile characteristics of AZ61/B_4C nanocomposites

Composites	Ultimate tensile strength (MPa)	Yield strength (MPa)	Elongation (%)
A	158	101	10.4
B	166	114	8.6
C	178	126	6.8
D	194	138	5.6
E	182	129	6.0

Where ρth theoretical density and ρex is experimental density.

Plastic deformation and grain boundary diffusion are the two factors that have the most influence on the densification of magnesium-based composites [40]. The incorporation of B_4C nanoparticles into the composites resulted in a slight improvement in the performance of these two processes: The AZ61 composites had10 wt%, and B_4C had a density of 1.830 g/cm^2, which was higher than that of the composites containing 2.5 wt%. Porosities of less than 2% throughout the magnesium metal matrix nanocomposites are considered to be within the acceptable range for these composites. Because AZ61 and the reinforced particulates used in the stir casting process have lower surface tension, trapped air bubbles can flow into the molten mixture and escape during the process.

4.3. Mechanical properties

The values of the yield strength and tensile strength of the AZ61/B_4C nanocomposites were derived from the stress–strain curve using the results of the tensile test (Table 2). It was found that increasing the reinforcements in the composites led to an increase in their tensile properties up to 7.5wt% for nano-B_4C before the properties began to deteriorate. The increased ultimate tensile and yield strengths of the composites made with the use of B_4C nanoparticles may be attributed to grain purification that begins well under cooling from the reinforcements. Because the reinforcements are ductile and can therefore undergo plastic deformation, the bonding between the reinforcement particles and matrix makes it less likely for them to generate heavy stress gradients. Because of the difference in the plastic deformation characteristics between AZ61, which is ductile, and the reinforcements, which are hard and brittle, the limitation of the AZ61 matrix and the reinforcement nanoparticles may serve as a location for stress deliberation in the process of distinguishing the two.

The relationship between the AZ61/B_4C nanocomposites and their hardness levels is illustrated in Figure 4. It is evident from the information presented above that the weight percentage of reinforcement nanoparticles is directly correlated with the hardness of the material. When a soft and ductile matrix is combined with hard reinforcements, it leads to arise in the solidity of the base matrix. An appropriate stir casting process results in an even distribution of reinforcements, which contributes to the high solidity of composites containing 7.5 wt% B_4C. When B_4C nanoparticles comprise more than 7.5 wt% of the matrix, the hardness of the composites is reduced because the particles group together. The porosity range in all AZ61/B_4C nanocomposites

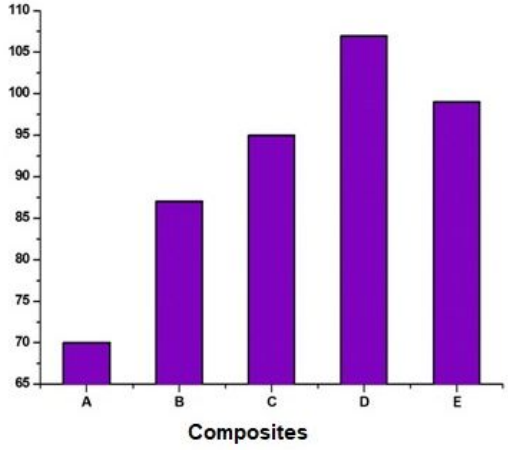

Fig. 4. AZ61/B_4C nanocomposites and the hardness of their relationship

was extremely low, and the effect was stable with regard to the composites' hardness. As a result of the increase in the percentage of reinforcement to above 7.5wt%, agglomeration occurred, which results in the reduction of hardness for AZ61/10wt.%B_4C nanocomposites (Figure 2e).

In addition, the results obtained for the compressive and tensile strengths of the AZ61/B_4C composites were the same as those obtained for the hardness difference for the different weight percentages of B_4C nanoparticles. The Orowan mechanism is one of the most effective ways to strengthen B_4C composites with a magnesium matrix.

Figure 5 shows the range of the compressive strength values and the stress-strain curve of AZ61/B_4C nanocomposites. The compressive strength increased up to 7.5 wt% with the nano-B_4C reinforcements until it reached 350MPa, after which it began to decrease. The load-bearing capacity of the AZ61/B_4C nanocomposites improved and the compressive strength increased because of their resistance to crack propagation. When the nanocomposites contain 10wt% B_4C, the cluster formation of the reinforcement particles results in nanocomposites with lower compressive strength, as shown in the SEM pictures in Figure 2e. According to the Hall–Petch equation [24], an increase in UCS is proportional to the inverse proportion of grain size to strength.

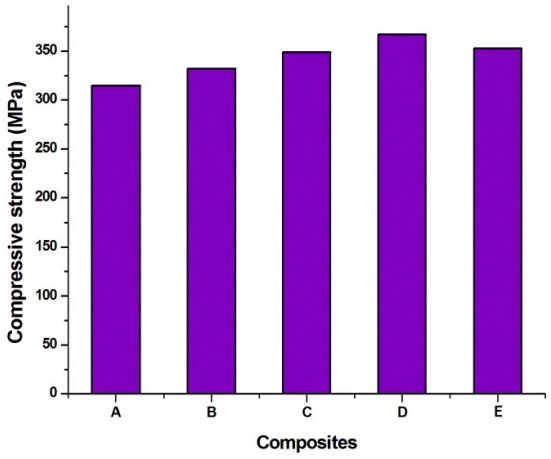

(A)

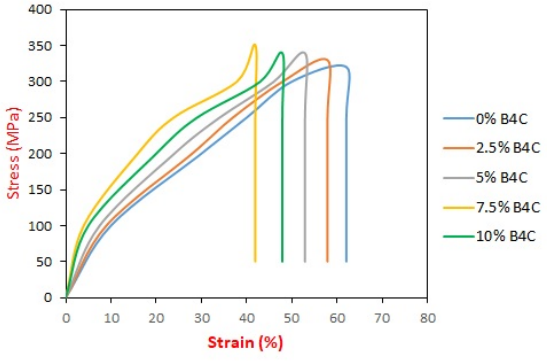

(B)

Fig. 5. (a) AZ61/B_4C nanocomposites and the compressive strength of their relationship (b) stress-strain curve of AZ61/B_4C nanocomposites

Figure 6 displays the findings of the tests conducted to determine the strike strength of the AZ61/B_4C nanocomposites. On the basis of these findings, the impact strength of the AZ61/B_4C nanocomposites was 18.5 J, 22.1 J, 26.9 J, and 25.8 J when there was 2.5 wt%, 5 wt%, 7.5 wt%, and 10 wt% of B_4C nanoparticles in the matrix, respectively. The presence of nano-B_4C reinforcements, which is a material that is equally as ductile as AZ61 but more difficult, is credited with improving the impact strength of the material. Because B_4C nanoparticles already have some ductility built into them, the AZ61 matrix composite has inherent toughness. The impact strength of the nanocomposites containing 10 wt% B_4C decreased, which

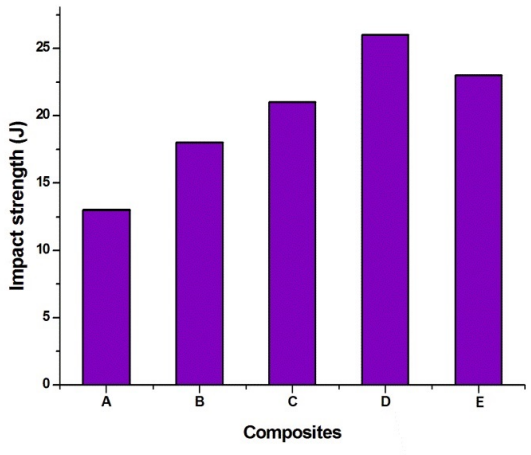

Fig. 6. AZ61/B_4C nanocomposites and the impact strength of their relationship

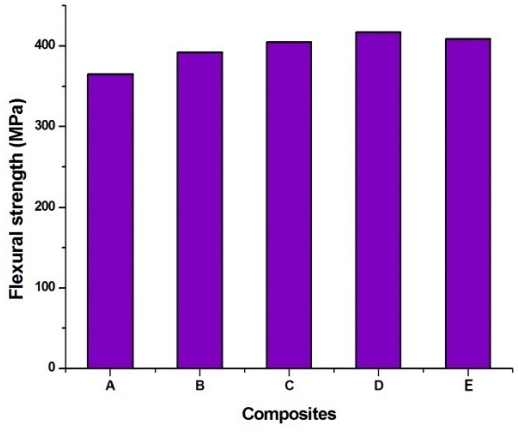

Fig. 7. AZ61/ B_4C nanocomposites and the flexural strength of their relationship

is not surprising given that nano-B_4C is naturally a soft and fairly brittle material. It fractured in a ductile-brittle mode, which is attributable to the presence of nano-B_4C components.

Figure 7 depicts the flexural strength values that were determined to have been achieved by the AZ61/B_4C nanocomposites. This clearly shows the gradual increase of reinforcement nanoparticles, which then began to decrease at 10% B_4C weight. The enhanced flexural strength was attributed to the AZ61's finer nanoparticles in the reinforcement. After the AZ61 material hardened, the precipitation of Mg2Si intermetallic particles could be regulated. The heterogeneous circulation of AZ61 with B_4C nanoparticles, poor ductility, and the formation of microcracks all contributed to a decrease in the flexural strength of the composites.

4.4. Corrosion properties

The corrosion test was used to investigate the deterioration process that occurs in the component while it is submerged in the solution. If corrosion current density (I_{corr}) decreases, the rate of corrosion will decrease, but the material will be more resistant to corrosion. The incorporation of nanoparticles into the composite led to an increase in the resistance of the material to corrosion. The value of I_{corr} continued to decrease until it reached 7.5 wt% of the nanocomposites, after which it began to rise. This reflects the high bonding of reinforcement in the magnesium and the effect of nano-B_4C addition; the best nanocomposites have a low Icorr value, and the best composites have 7.5 wt% of that reinforcement. Compared to sample D, the Icorr value produced by sample E is lower, indicating that an increased amount of reinforcement leads to a decreased level of bonding with the magnesium matrix.

Table 3. Corrosion properties of the AZ61/B_4C nanocomposites

Composites	I_{corr} (mA/cm^2)	E_{corr} (mV)	Corrosion rate (mils/yr)
A	0.0039751	−753.15	355.37
B	0.0032398	−856.25	338.70
C	0.0030175	−869.60	320.96
D	0.0021956	−916.36	220.47
E	0.0024096	−909.77	240.36

The formula was used to determine the corrosion rate:

$$\text{Corrosion rate(mpy)} = \frac{0.13 \times I_{corr} \times Ew}{\rho}$$

Where I_{corr} is the corrosion current density (μA/cm^2); Ew is the equivalent weight of AZ61/B_4C nanocomposite material; and ρ is density (g/cm^3) of the AZ61/B_4C nanocomposite material.

Table 4. Experimental results

Exp. No.	Wt% B_4C	L (N)	SV (m/s)	SD (m)	WR (mm^3/m)	COF
1	0	4	1	400	0.0084	0.482
2	0	8	2	800	0.0076	0.526
3	0	12	3	1200	0.0087	0.489
4	0	16	4	1600	0.0097	0.561
5	2.5	4	2	1200	0.0049	0.597
6	2.5	8	1	1600	0.0075	0.606
7	2.5	12	4	400	0.00672	0.685
8	2.5	16	3	800	0.00789	0.587
9	5	4	3	1600	0.0031	0.774
10	5	8	4	1200	0.0045	0.695
11	5	12	1	800	0.0051	0.763
12	5	16	2	400	0.0068	0.79
13	7.5	4	4	800	0.0031	0.585
14	7.5	8	3	400	0.0039	0.493
15	7.5	12	2	1600	0.0048	0.521
16	7.5	16	1	1200	0.00501	0.566

Abbreviations: L, load; SV, sliding velocity; SD, sliding distance, WR, wear rate, COF, coefficient

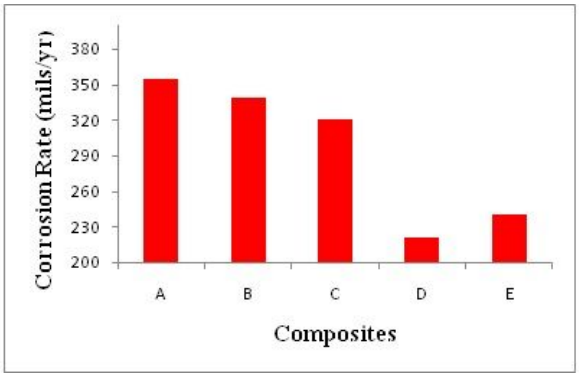

Fig. 8. AZ61/B_4C nanocomposites and the corrosion behavior of their relationship

4.5. Tribological behavior

The tribological behavior study was performed according to the L16 orthogonal array to forecast the optimum process parameters by Grey relational analysis (GRA). The wear test was done with the process parameters B_4C wt% (0, 2.5, 5, and 7.5), load (4, 8, 12, and 16 N), sliding velocity (1, 2, 3, and 4 m/s), and sliding distance (400, 800, 1200,and1600m) to find the optimum parameters to attain the least wear rate and coefficient of friction. The results are shown in Table 4.

4.5.1. The result of various task parameters on WR

Figures (9–11) show the contour plot for WR. Figure 9 shows the nano-B_4C weight percentage vs. load. It was obviously revealed that the wear rate progressively increases with an increase in load at any sliding velocity (SV) and distance. It was demonstrated that the least wear rate (WR) was attained at the lowest level of load (L). Figure 10 shows the nano-B_4C weight percentage versus sliding velocity. It was found that a higher value of sliding distance (SD) produces more wear rate in spite of more contact between the sample and counter disc. The highest wear rate was attained with a higher value for sliding distance. Figure 11 shows the nano-B_4C weight percentage versus sliding distance. Sliding velocity was a minor variable, which means the response of wear rate doesn't depend on that parameter. Though the upper value of sliding distance increases the wear rate at any sliding velocity continued constant. It was clearly perceived that low wear rate was attained at the mid-level of sliding and sliding distance. From the contour plot in Figures (9–11), it can be seen that an elevation in L, SV, and SD enhances the WR, and a reduction was observed when increasing the weight percent

of nano-B_4C reinforcement. Figures (9–11) clearly show the effects of the nano-B_4C weight percent has better wear resistance than that of other parameters. 7.5 wt% nano-B_4C. This could be because the nano-B_4C particles act as a barrier to protect against surface defoliation, resulting in improved WR. The WR decreases as the weight percent of nano-B_4C decreases (7.5 >5 >2.5 >0 wt%). When nano-B_4C weight percent decreases, the formation of frictional heat minimizes the hardness of composites, which ultimately results in a decline in the WR.

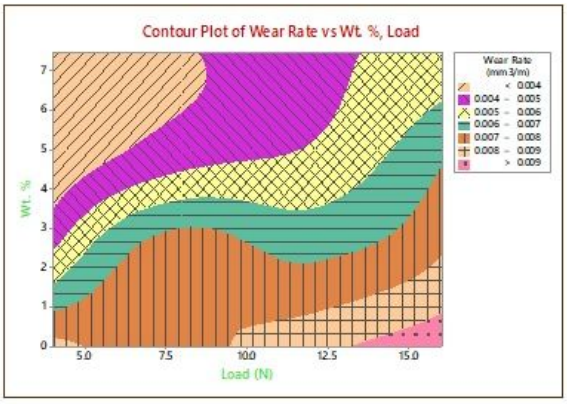

Fig. 9. Contour plot: wt% B_4C vs. load

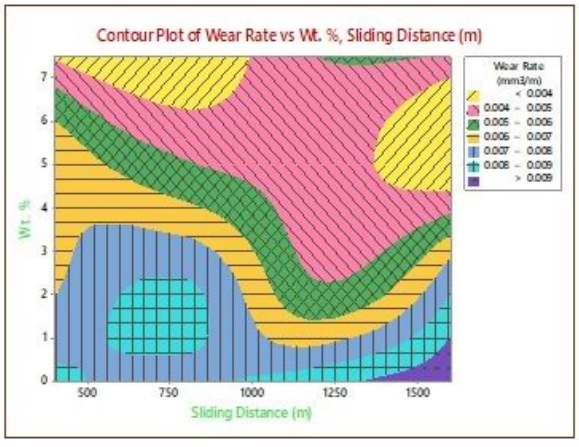

Fig. 10. Contour plot: wt% B_4C vs. sliding distance

4.5.2. Effects of various task parameters on coefficient

The contour plots for the coefficient (COF) in Figure 12 represent weight percent versus load. It is

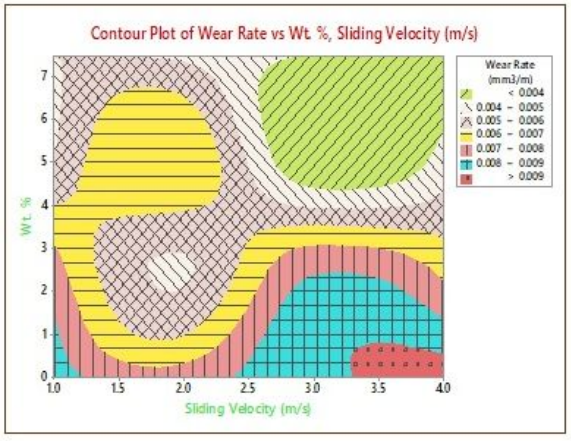

Fig. 11. Contour plot: wt% B_4C vs. sliding velocity

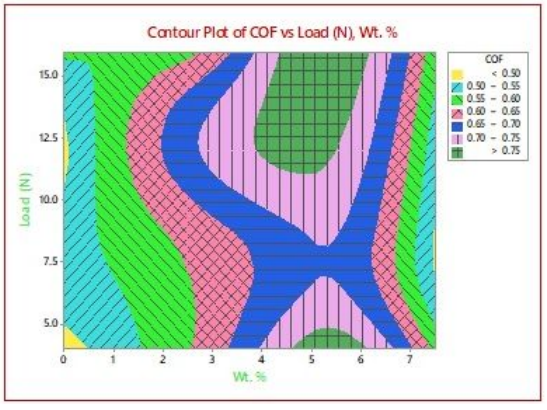

Fig. 12. Contour plot: wt% B_4C vs. load

clear that the COF progressively increases with increase in load at any sliding velocity and distance. The lowest COF was obtained at the lowest level of load. Figure 13 shows weight percent versus sliding distance. It was revealed that a greater value of sliding distance produces the maximum COF because there is more contact between the specimen and the counter disc. The maximum COF was attained with greatest value for sliding distance. Figure 14 shows weight percent versus SD. This result shows that the sliding velocity was an insignificant variable, that is, the response of COF doesn't depend on this parameter. The finding that higher values of sliding distance increase the wear rate at any sliding velocity remained constant. It was clear that a low COF was attained at the mid-level of sliding velocity and

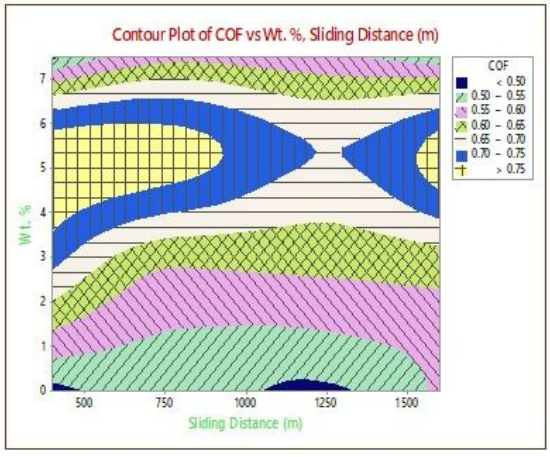

Fig. 13. Contour plot wt% B_4C vs. sliding distance

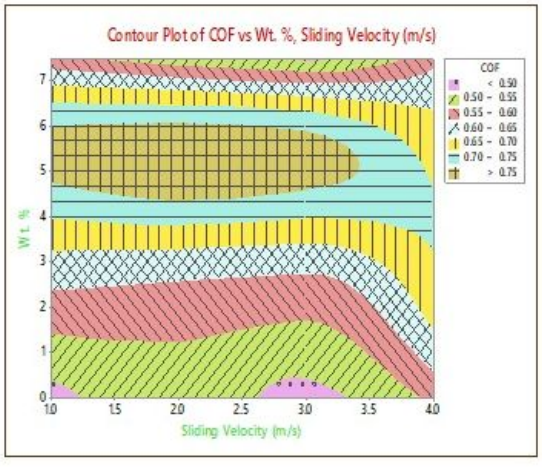

Fig. 14. Contour plot wt% B_4C vs. sliding velocity

sliding distance. As can be seen in Figures (12–14), the COF value decreases as the weight percent of B_4C nanoparticles, L, SV, and SD increase. It is possible that the primary reason for the decrease in COF is that, as the load continues to increase, the temperature of the worn surface continues to rise, which causes the alloys to become more pliable. The COF decreased as the weight percentage of B_4C nanoparticles reached its maximum, which occurred at 7.5 wt%. The scattering of particles is consistent, which results in a lower value compared to the various composites.

4.5.3. Grey relational examination

The Taguchi process, which is connected to Grey, is a useful method. It is possible to achieve desirable process parameters by converting multi-response inspection into a tool-based, one-response optimization using Grey. The steps involved in GRA are outlined below. The initial step is to standardize the control values that have been collected. The Taguchi method can be used to improve performance characteristics. Table 5 presents the calculated S/N ratio and the normalized S/N ratio values for the smallest possible increase in WR and COF. The GRC, GRG, and ranks for all the 16 trials are presented in Table 6. The GRG developed is shown in the first rank of Table 6, which indicates that it has improved capabilities for multiple executions. According to Table 6, the parameters found in the twelfth experiment are the most optimal for a wide variety of performance characteristics, including the WR and COF. The response table for GRG is displayed in Table 7. It can be deduced from Table 7 that the maximum value for the maximum to minimum esteem range was 4.262. As a result, it is common knowledge that the weight percentage of nano-B_4C is the most important factor in determining WR and CO flag, followed by L, SV, and SD. The series of stimulating influences is in the following order: B_4C (4.262), L (1.925), SV (01.062), and SD (0.46). The GRG is illustrated in Figure 8. The plots of the main effects for GRG are shown in Figures 15 and 17. The following steps are used to find optimal results.

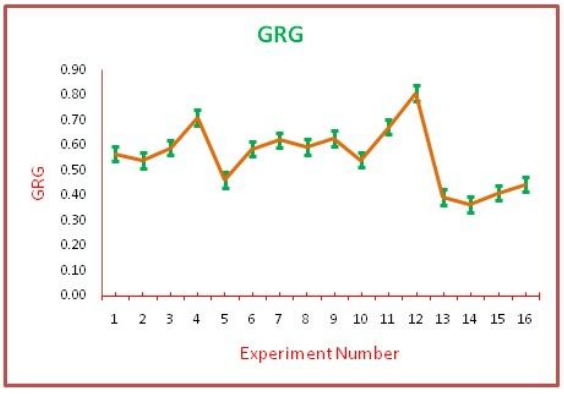

Fig. 15. Grey relational grade

Table 5. Calculated S/N ratio as well as the normalized S/N ratio

S/N ratio for wear	S/N ratio for COF	Normalization for wear	Normalization for COF
41.5144	6.3391	0.874	0.000
42.3837	5.5803	0.786	0.177
41.2096	6.2138	0.905	0.029
40.2646	5.0207	1.000	0.307
46.1961	4.4805	0.401	0.433
42.4988	4.3505	0.775	0.463
43.4526	3.2862	0.678	0.711
42.0585	4.6272	0.819	0.399
50.1728	2.2252	0.000	0.959
46.9357	3.1603	0.327	0.741
45.8486	2.3495	0.436	0.930
43.3498	2.0475	0.689	1.000
50.1728	4.6569	0.000	0.392
48.1787	6.1431	0.201	0.046
46.3752	5.6632	0.383	0.157
46.0032	4.9437	0.421	0.325

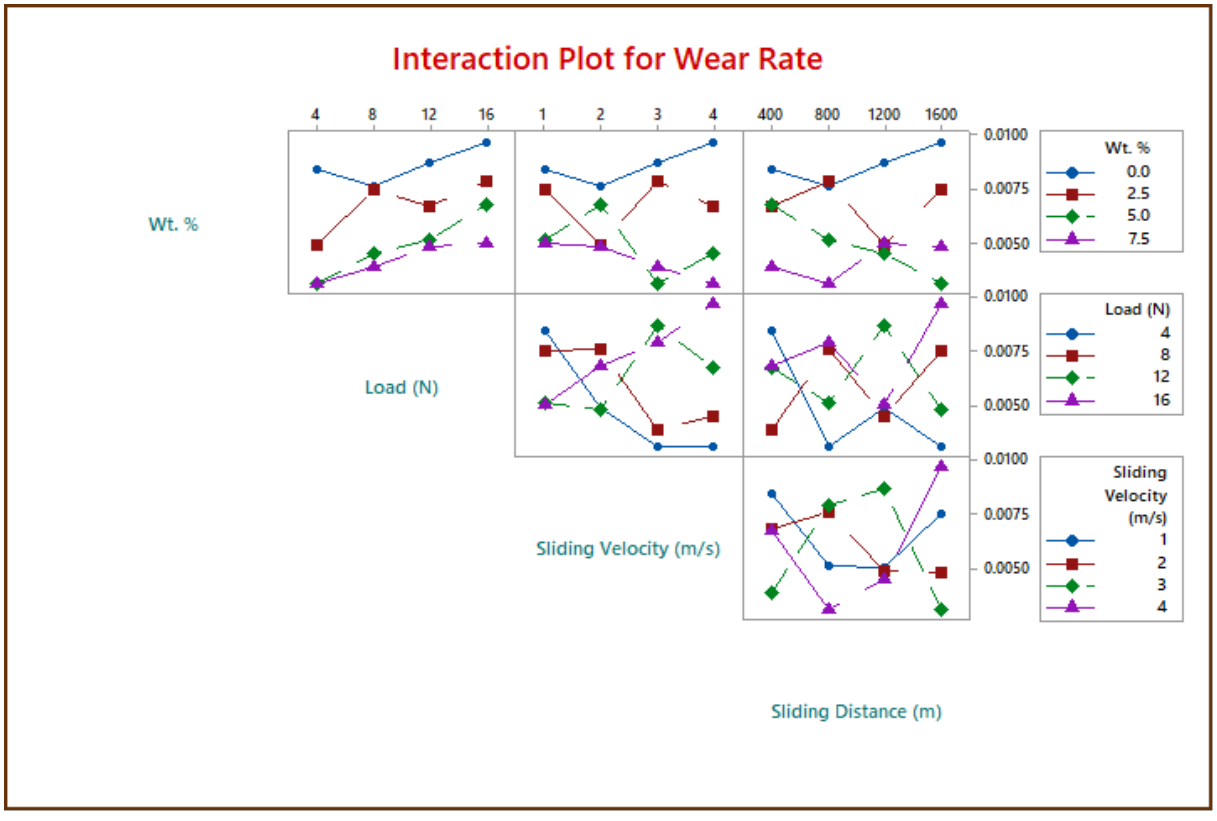

Fig. 16. Main effect plot for wear rate

Step 1. Calculate the value of the signal-to-noise ratio(S/N) for wear and COF:

$$\text{S/N ratio} = -\log_{10}\left(\sum_{i=1}^{n}\frac{yi\,(x)^2}{n}\right)$$

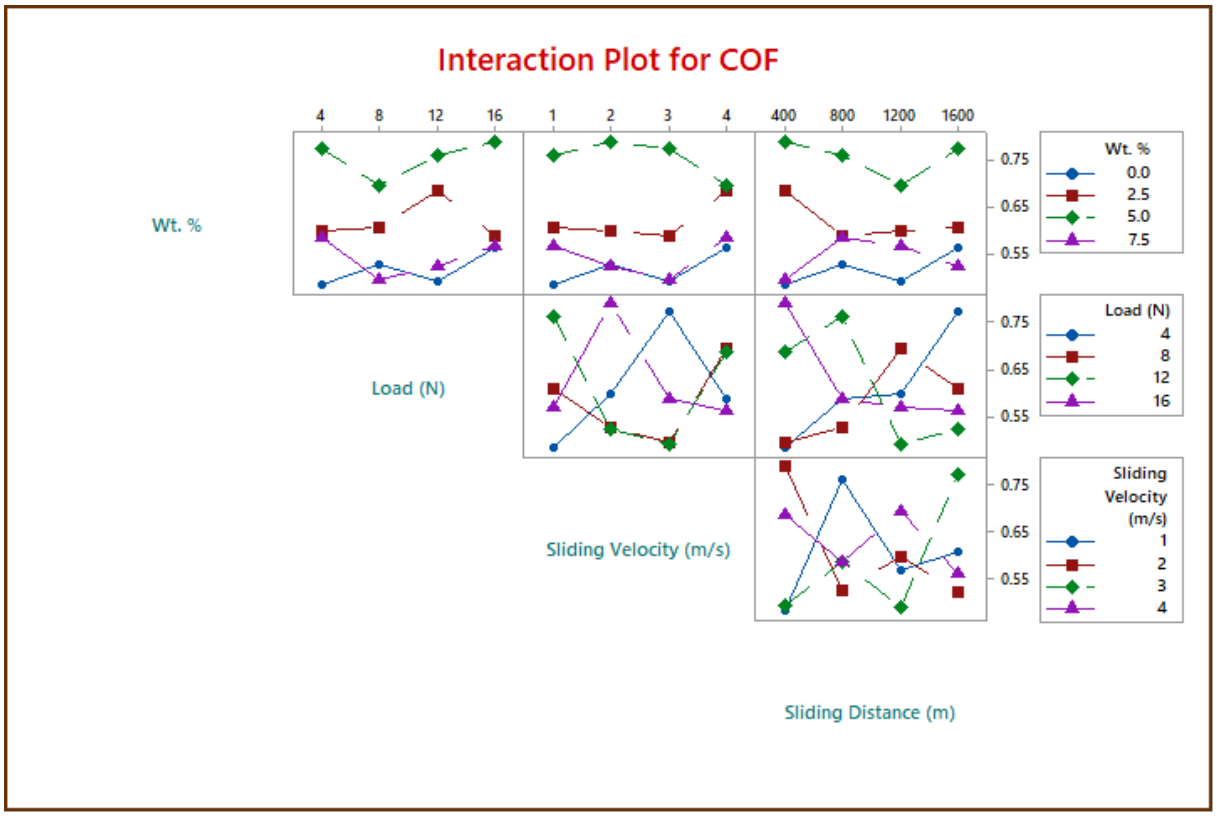

Fig. 17. Main effect plot for coefficient

Table 6. Calculated deviation sequences for GRC and GRG

Deviation sequence for wear	Deviation sequence for COF	GRC for wear	GRC for COF	GRG	Rank
0.126	1.000	0.799	0.333	0.566	9
0.214	0.823	0.700	0.378	0.539	11
0.095	0.971	0.840	0.340	0.590	7
0.000	0.693	1.000	0.419	0.710	2
0.599	0.567	0.455	0.469	0.462	12
0.225	0.537	0.689	0.482	0.586	8
0.322	0.289	0.608	0.634	0.621	5
0.181	0.601	0.734	0.454	0.594	6
1.000	0.041	0.333	0.924	0.628	4
0.673	0.259	0.426	0.658	0.542	10
0.564	0.070	0.470	0.877	0.673	3
0.311	0.000	0.616	1.000	0.808	1
1.000	0.608	0.333	0.451	0.392	15
0.799	0.954	0.385	0.344	0.364	16
0.617	0.843	0.448	0.372	0.410	14
0.579	0.675	0.463	0.426	0.444	13

Table 7. Grey relational grade response table

Level	Wt%	L (N)	SV (m/s)	SD (m)
1	4.469	5.954	5.017	4.925
2	5.003	6.024	5.417	5.363
3	3.659	4.974	5.478	5.913
4	7.921	4.099	5.139	4.851
Delta	4.262	1.925	0.46	1.062
Rank	1	2	4	3

Table 8. ANOVA for Grey relational grade

Source	DF	Adj SS	Adj MS	F Value	P Value	Contribution %
Wt%	3	0.148176	0.049392	16.67	0.022	67.19
L (N)	3	0.045723	0.015241	5.14	0.106	20.73
SV (m/s)	3	0.001433	0.000478	0.16	0.916	0.65
SD (m)	3	0.016302	0.005434	1.83	0.315	7.39
Error	3	0.008889	0.002963			
Total	15	0.220523				

Step 2. Calculate the value of the normalization for wear and COF:

$$y_i*(x) = \frac{\max z_i(y) - z_i(y)}{\max z_i(y) - \min z_i(y)}$$

Step 3. Determine the deviation sequence for wear and COF:

$$\xi_i(k) = \frac{\Delta\min + p\Delta\max}{\Delta x_i(k) + p\Delta\max}$$

Step 4. Determine the Grey relational coefficient (GRC) values for wear and COF:

$$\gamma_{pre} = \gamma_m + \sum_{k=1}^{n} (\gamma_i - \gamma_m)$$

Step 5. Calculate the average of the GRC values for wear and COF. These values are Grey relational grade (GRG) values. The greater the GRG value, the better the possibility of finding the best alternative.

Step 6. Use GRG values to rank the alternative parameter.

4.5.4. Variance analysis

Analysis of variance (ANOVA) was used to investigate the outcome of the process parameters that caused abundant dominance features. The results of the ANOVA for GRG can be found in Table 8, which helps identify the factors that have the greatest impact. Table 8 shows that the weight percentage of nano-B_4C is the most important factor (contributing 67.19%), and it does have the greatest influence on the multi-enactment properties of AZ61/B_4C nanocomposites, followed by L (20.73%), SD (7.39%), and SV (0.65%).

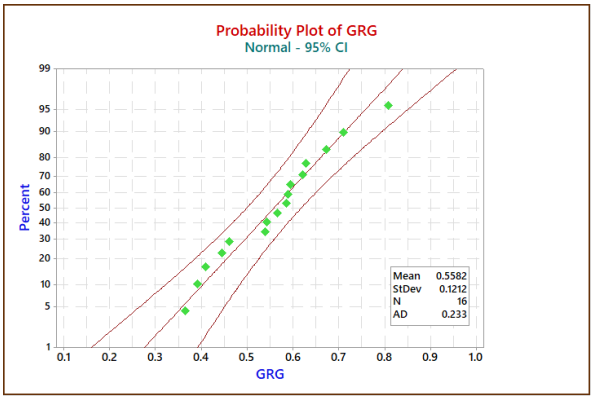

Fig. 18. Normal probability plot

5. Conclusions

- Different nano-B_4C reinforcement weight percentages (2.5, 5, 7.5, and 10wt%)

were successfully used in the production of AZ61/B_4C nanocomposites. Composites were manufactured using stir casting and after they were made, the influence of B_4C nanoparticles on the mechanical, corrosion, and tribological properties of the composites was studied.

- Scanning electron micrographs displayed that the reinforcements were evenly dispersed throughout the AZ61 matrix. This is because of the robust interfacial connections.
- As more nano-B_4C reinforcement was added to the matrix, the density of the composites improved.
- Up to 7.5 weight percent of B_4C nanoparticles, corrosion and the mechanical parameters of the composites, such as hardness, impact, tensile, compressive, and flexural strength, increased. However, after that, they deteriorated.
- A pin-on-disc tribometer was used to investigate the influence of nano-B_4C reinforcement on the tribological behavior of AZ61 composites under different tribological parameters.
- AZ61/B_4C nanocomposites are suitable for defining the finest task parameters to accomplish the less WR and COF values. GRA was utilized to inspect the tribological properties of the AZ61/B_4C nanocomposites. The best parameters for obtaining the nominal WR and COF were 7.5wt% B_4C, L = 20 N, SV = 3 m/s, and SD = 400 m.
- ANOVA was performed to find the parameters that had an effect on the WR and COF responses. The percentage of the GRG calculated value was determined to be 83.3%.

References

[1] Luo XC, Zhang DT, Zhang WW, Qiu C, Chen DL.Tensile properties of AZ61 magnesium alloy produced by multi-pass friction stir processing: effect of sample orientation. Mater Sci Eng A.2018; 725:398–405. https://doi.org/10.1016/j.msea.2018.04.017

[2] Singh K, Singh G, Singh H. Investigation of microstructure and mechanical properties of friction stir welded AZ61 magnesium alloy joint. J Magnes Alloys.2018;6(3):292–8. https://doi.org/10.1016/j.jma.2018.05.004

[3] Dai Y, Chen X-H, Yan T, Tang A-T, Zhao D, Luo X, Liu C-Q, Cheng R-J, Pan F-S. Improved corrosion resistance in AZ61 magnesium alloys induced by impurity reduction Acta MetalSin (Engl Lett). 2020; 33(2):225–232. https://doi.org/10.1007/s40195-019-00914-2

[4] Hilšer O, Rusz S, Tański T, Snopiński P, Džugan J, Kraus M. Mechanical properties and structure of AZ61 magnesium alloy processed by equal channel angular pressing. IOP Conf Ser Mater Sci Eng. 2017; 179(1):012028. https://doi.org/10.1088/1757-899X/179/1/012028

[5] Singh K.Singh G, Singh H. Investigation on the microstructure and mechanical properties of a dissimilar friction stir welded joint of magnesium alloys. Proc Inst Mech Eng L-J Mat. 2019; 233(12):2444–54. https://uk.sagepub.com/en-gb/journals-permissions

[6] Öteyaka MÖ, Ghali E, Tremblay R. Corrosion behaviour of AZ and ZA magnesium alloys in alkaline chloride media. Int J Corros.2012;110. https://doi.org/10.1155/2012/452631

[7] Li L, Nam ND. Effect of yttrium on corrosion behavior of extruded AZ61 Mg alloy. J Magnes Alloys. 2016; 4(1):44–51. http://dx.doi.org/10.1016/j.jma.2015.11.008

[8] Moheimani, SK, Keshtgar A, Khademzadeh K, Tayebi M, Rajaee A, Saboori A. Tribological behaviour of AZ31 magnesium alloy reinforced by bimodal size B_4C after precipitation hardening, J Magnes Alloys. 2021; 4:38. https://doi.org/10.1016/j.jma.2021.05.016

[9] Dziubińska A, Gontarz A, Horzelska K, Pieśko P. The microstructure and mechanical properties of AZ31 magnesium alloy aircraft brackets produced by a new forging technology. Procedia Manuf. 2015; 2:337–41. https://doi.org/10.1016/j.promfg.2015.07.059

[10] Dinaharan I, Zhang S, Chen C, Shi Q. Assessment of Ti-6Al-4V particles as reinforcement for AZ31 magnesium alloy-based composites to boost ductility incorporated through friction stir processing. J Magnes Alloys.2022; 10:979–92. https://doi.org/10.1016/j.jma.2020.09.026

[11] Singh A, Bala N. Fabrication and tribological behavior of stir cast Mg/B_4C metal matrix composites.Metall Mater Trans A. 2017; 48(10):5031–45. https://doi.org/10.1007/s11661-017-4203-x

[12] Ramanujam N, Muthukumaran S, Rao NB, Ramarao M, Mangrulkar AL, AliAKS, Pugazhendhi L, Markos M. Experimental investigations on mechanical properties of AZ31/eggshell particle-based magnesium composites. Adv. Mater Sci Eng. 2022; 1–7. https://doi.org/10.1155/2022/4883764

[13] Kumar KCK, Kumar BR, Rao NM.Microstructural,

mechanical characterization, and fractography of AZ31/SiCreinforced composites by stir casting method. Silicon. 2021; 14:5017–27. https://doi.org/10.1007/s12633-021-01180-7

[14] Marimuthu M, Berchmans JL. Preparation and characterization of B_4C particulate reinforced Al-Mg alloy matrix composites. Int J Mod Eng Res. 2013;3(6):1419. http://www.ijmer.com/papers/Vol3_Issue6/CG3637233729.pdf

[15] Kaya AA, Kayali ES, Eliezer D, Gertsberg G, Moscovitch N. Addition of B_4C to AZ91 via die casting and its effect on wear behavior. Mater Sci Forum. 2005;488:741–4. http://dx.doi.org/10.4028/www.scientific.net/MSF.488-489.741

[16] Turan ME, Zengin H, Cevik E, Sun Y, Turen Y, Ahlatci H. Wear behaviors of B_4C and SiC particle reinforced AZ91 magnesium matrix metal composites. Int J Mater Metall Eng. 2016; 10(9):1224–1227. https://zenodo.org/record/1126900/files/10005559.pdf

[17] Gupta M, Wong WLE. Magnesium-based nanocomposites: lightweight materials of the future. Mater Charact. 2015; 105:30–46. http://dx.doi.org/10.1016/j.matchar.2015.04.015

[18] Matta AK, Koka, NSS, Devarakonda SK. Recent studies on particulate reinforced AZ91 magnesium composites fabricated by stir casting — a review. J Mech Energy Eng. 2020; 4(44):115–26. https://doi.org/10.30464/jmee.2020.4.2.115

[19] Çevik E, Gündoğan M, İncesu A, Turan M E. Corrosion behavior of grapheme nano platelet-coated TiB2 reinforced AZ91 magnesium matrix semi-ceramic hybrid composites. Hittite J Sci Eng. 2021; 8(1):27–33. https://doi.org/10.17350/HJSE19030000209

[20] Kulisz M, Zagórski I, Korpysa J. The effect of abrasive waterjet machining parameters on the condition of Al-Si alloy.Materials.2020; 13(14):3122. http://dx.doi.org/10.3390/ma13143122

[21] Huang SJ, Subramani M, Chiang CC. Effect of hybrid reinforcement on microstructure and mechanical properties of AZ61 magnesium alloy processed by stir casting method. Compos Commun.2021; 25:100772. https://doi.org/10.1016/j.coco.2021.100772

[22] Sathish T, Mohanavel V, Ansari K, Saravanan R, Karthick A, Afzal A, Alamri S, Saleel CA. Synthesis and characterization of mechanical properties and wire cut EDM process parameters analysis in AZ61 magnesium alloy + B_4C + SiC, Materials. 2021;14(13):3689. https://doi.org/10.3390/ma14133689

[23] Ye HZLiu XY. Review of recent studies in magnesium matrix composites.J Mater Sci. 2004; 39(20):6153–71. https://doi.org/10.1023/B:JMSC.0000043583.47148.31

[24] Jalilvand MM, Mazaheri Y. Effect of mono and hybrid ceramic reinforcement particles on the tribological behavior of the AZ31 matrix surface composites developed by friction stir processing. Ceram Int. 2020; 46(12):20345–56. https://doi.org/10.1016/j.ceramint.2020.05.123

[25] Titarmare V, Banerjee S, Sahoo P. Fabrication and characterization of AZ31-B_4C composites. Mater Today Proc 2022; 59(1):153–60. https://doi.org/10.1016/j.matpr.2021.10.373

[26] Zhou H,Zhang C, Han B, Qiu J, Qin S, Gao K, Liu J, Sun S, Zhang H. Microstructures and mechanical properties of nanocrystalline AZ31 magnesium alloy powders with submicron TiB2 additions prepared by mechanical milling.Crystals.2020;10(6):550. https://doi.org/10.3390/cryst10060550

[27] Yao, Y-T, Jiang L, Fu G-F, Chen L-Q, Wear behavior and mechanism of B_4C reinforced Mg-matrix composites fabricated by metal-assisted pressure less infiltration technique. Trans Nonferrous Met Soc China. 2015; 25(8):2543–8. https://doi.org/10.1016/S1003-6326(15)63873-0

[28] Paramsothy M, Hassan SF, Srikanth N, Gupta M. Simultaneous enhancement of tensile/compressive strength and ductility of magnesium alloy AZ31 using carbon nanotubes. J Nano sci Nanotechnol. 2010; 10(2):956–64. https://doi.org/10.1166/jnn.2010.1809

[29] Aydin F, Yavuz S, EmreTuran M. Influence of TiC content on mechanical, wear and corrosion properties of hot-pressed AZ91/TiC composites. J Compos Mater. 2020; 54(2): 141–52. https://doi.org/10.1177%2F0021998319860570

[30] Subramani M, Huang S-J, Borodianskiy K. Effect of SiC nanoparticles on AZ31 magnesium alloy. Materials. 2022; 15(3):1004. https://doi.org/10.3390/ma15031004

[31] El-Morsy A-W, Abouel-Kasem A.Tribological characteristics of deformed magnesium alloyAZ61 under dry conditions. J Tribol. 2011; 133/041603-1. https://doi.org/10.1115/1.4004761

[32] Yan H, Wan J, Nie Q. Wear behavior of extruded nano-SiCpreinforced AZ61 magnesium matrix composites. Adv Mech Eng. 2013(5), Article ID 489528, 1–5 pages. https://doi.org/10.1155/2013/489528

[33] Akkoyun F, Ercetin A. Automated grain counting for the microstructure of Mg alloys using an image processing method. J Mater Eng Perform.2022; 31:2870–7. https://link.springer.com/article/10.1007/s11665-021-06436-2

[34] Niraj N, Pandey KM, Dey A.Tribologicalbehaviour of magnesium metal matrix composites reinforced with fly ash cenosphere. Mater Today Proc. 2018;5(9):Part 3, 20138-20144. https://www.sciencedirect.com/science/article/abs/pii/S2214785318315098

[35] Lim CYH, Lim SC, Gupta M. Wear behaviour of SiCp-reinforced magnesium matrix composites. Wear. 2003;255(1–6):629–37. https://www.sciencedirect.com/science/article/abs/pii/S0043164803001212

[36] Santhosh MS, Natrayan L, Kaliappan S, Patil PP, Rao YS, Kumar TNS, Dhanraj JA, Paramasivam P. Mechani-

cal and wear behavior of nano-fly ash particle-reinforced Mg metal matrix composites fabricated by stir casting technique. J Nanomater. 2022;2022:1–8, https://www.hindawi.com/journals/jnm/2022/5465771/

[37] Singh H, Kumar D, Singh H. Development of magnesium-based hybrid metal matrix composite through in situ micro, nano reinforcements, J Compos Mater. 2020;55(1):109–23. https://journals.sagepub.com/doi/full/10.1177/0021998320946432

[38] Ercetin A. Application of the hot press method to produce new Mg alloys: characterization, mechanical properties, and effect of Al addition. J Mater Eng Perform.2021;30:4254–62. https://link.springer.com/article/10.1007/s11665-021-05814-0

[39] Ercetin A, Akkoyun F, Simsir E, Pimenov DY, Giasin K, Chandrashekarappa MPG, Lakshmikanthan A, Wojciechowski S.Image processing of Mg-Al-Sn alloy microstructures for determining phase ratios and grain size and correction with manual measurement.Materials. 2021; 14(5095):1–16. https://doi.org/10.3390/ma14175095

[40] Jayakumar K, Mathew J, Joseph MA, Kumar RS, Shukla AK, Samuel MG. Synthesis and characterization of A356-SiCp composite produced through vacuum hot pressing. Mater Manuf Process. 2013; 28(9):991–8. https://doi.org/10.1080/10426914.2013.773012

Received 2023-01-28
Accepted 2023-07-17